Design and optimization of fractional slot concentrated winding PM vernier motor

Design and Optimization of Fractional Slot Concentrated Winding PM Vernier Motor

Nima Arish*, Achmad Z. Dramat, Maarten J. Kamper, Rong-Jie Wang and Mabala Phumudzo
Department of Electrical and Electronic Engineering, Stellenbosch University, South Africa
*nima.arishh@gmail.com, azdramat11@gmail.com, kamper@sun.ac.za, rwang@sun.ac.za, mabalaphumudzo@gmail.com

***Abstract*—The Permanent Magnet Vernier Motor (PMVM) is a novel type of permanent magnet motor that has attracted considerable attention in recent years due to its ability to directly connect to the load. It exhibits remarkable efficiency across a wide range of speeds by employing the modulation effect, a technique that intentionally mismatches rotor and stator poles to enhance power density. This paper explores the design, analysis, and optimization of a 4.2 kW low pole ratio Fractional Slot Concentrated Winding Permanent Magnet Vernier Motor (FSCWPMVM) with a coil pitch of 2. The optimization process utilizes the NSGA algorithm to minimize motor mass while maintaining acceptable performance. The analysis employs the Finite Element Method (FEM) to evaluate torque, efficiency (EF), losses, power factor (PF), forces, demagnetization, mechanical, and thermal considerations.**

***Index Terms*—demagnetization, modulation effect, mmf harmonic, pole-ratio, pm vernier motor, thermal analysis.**

I. Introduction

The relentless pursuit of sustainable and efficient propulsion systems has driven the development of innovative electrical machine topologies. While conventional methods possess certain advantages, they are often constrained by inefficiencies and environmental concerns. This has necessitated the exploration of novel electrical machine topologies that offer enhanced energy efficiency, precise control, and adaptability to diverse operating conditions. Recent advancements in electrical machine technology have heralded the emergence of the PMVM, a promising member of the Permanent Magnet Synchronous Motor (PMSM) family. The PMVM has gained significant traction in the propulsion domain due to its ability to directly connect the shaft to the propeller, facilitating efficient and precise control of propulsion systems [1]. This direct coupling eliminates the need for gearboxes, resulting in higher power density and overall system efficiency [2]–[8].

This paper delves into the intricacies of PMVM technology, design principles, and performance characteristics. Furthermore, it explores the optimization of low pole ratio FSCWPMVM with a coil pitch of two. Employing the Non-Dominated Sorting Genetic Algorithm (NSGA) algorithm, the study aims to minimize motor mass while utilizing the FEM to evaluate air-gap flux density, back EMF, torque, efficiency, losses, unbalanced magnetic force, thermal considerations, and demagnetization.

This work was financially supported by the Department of Electrical and Electronic Engineering, Stellenbosch University in South Africa.

II. Operation Principle

The following section offers a mathematical exploration of the equations governing PMVM. In vernier machine theory, the performance metrics are determined by the number of rotor pole pairs p_r and the number of stator pole pairs p_s. The working principle of the vernier machine is based on the magnetic gear effect and the following equation has to be satisfied [3]

$$Q_s = p_r \pm p_s \tag{1}$$

where Q_s is the number of slots. The condition $Q_s = p_r - p_s$ leads to the magnetic armature field rotating in the opposite direction of the rotor, while the condition $Q_s = p_r + p_s$ causes them to rotate in the same direction as the rotor. Rotating in the same direction generally produces higher torque compared to the opposite direction, while rotating in the opposite direction can have lower ripple torque and cogging torque [10]. Therefore, this paper utilizes the $Q_s = p_r + p_s$ $(24 = 17 + 7)$ configuration for designing the vernier machine to achieve higher torque. Assuming infinite relative permeability and uniformly magnetized PMs, the air-gap flux density is derived as the product of the permeance function and the PM magnetomotive force (MMF) distribution.

$$P(\theta_s) = \sum_{i=1,3,5,\dots} P_0 F_i cos(ip_r\theta_s - i\omega t) \tag{2}$$

$$F_{PM}(\theta_s, t) = \sum_{i=1,3,5,\dots} P_1 F_i cos(ip_r\theta_s - i\omega t) cos(Q_s\theta_s) \tag{3}$$

After the assumption of uniform area the air-gap flux density can be calculated as

$$B_g(\theta_s, t) = P(\theta_s) F_{PM}(\theta_s, t)$$

$$= \sum_{i=1,3,5,\dots} \Bigg[P_0 F_i \cos(ip_r\theta_s - i\omega t) + \frac{P_1 F_i}{2} \cos\left((Q_s - ip_r)\theta_s + i\omega t\right) + \frac{P_1 F_i}{2} \cos\left((Q_s + ip_r)\theta_s - i\omega t\right) \Bigg] \tag{4}$$

As can be seen from the above equation, there are three terms. The first term is found in classical machine theory while the other two terms are produced by the modulation effect of the stator slots. By applying FFT to the radial and

tangential air-gap flux density of the PMVM with a gear ratio of 2.4, the active harmonics (p_r^{th}, $(Q_s - p_r)^{th}$, and $(Q_s + p_r)^{th}$), corresponding to their respective gear ratios and slot configurations, are identified in Fig 1, as described in equation (4).

III. Field-Circuit Design Approach

The study utilizes a coupled field-circuit model to analyze and evaluate the performance of a PMVM in steady-state operation. The output performance is calculated based on equations derived from the fundamental per-phase equivalent circuit as shown in Fig. 2(a). Key parameters include electromotive force (EMF) represented by E, phase resistance denoted by R_{ph}, terminal voltage represented by V_{ph}, and phase current signified by I_{ph}. To account for core and eddy-current losses, a shunt resistance, R_{ce}, is introduced. Additionally, L_w and L_e represent the main and end-windings, respectively.

$$V_{ph} = E + I_{ph}\left(\frac{d(L_w + L_e)}{dt}\right) + I_{ph}R_{ph} \tag{5}$$

The dq-axis rotor reference frame is employed to simplify the analysis of machine performance over time. To facilitate dq-transformation, a reference phase is aligned with the rotor's positive d-axis. Adjusting the armature current angle achieves the desired torque. A PMVM in the dq-reference frame exhibits zero d-axis current and maximum q-axis current, corresponding to maximum torque. The steady-state dq-axis equivalent circuits for PMVM in the dq-axis reference frame can be derived from Fig. 2(b) and (c) based on the $I_d = 0$ strategy.

$$V_d = -\omega_r \lambda_q + \omega_r L_e I_q \tag{6}$$

$$V_q = \omega_r \lambda_d + R_{ph} I_q \tag{7}$$

The torque (T), real power (P), reactive power (Q) and PF for a PMVM in the dq-axis frame can be calculated as

$$T = \frac{3}{2} G_r p_s (\lambda_d I_{q1} - \lambda_q I_{d1}) \tag{8}$$

$$P = \frac{3}{2}(V_q I_q) \tag{9}$$

$$Q = \frac{3}{2}(V_d I_q) \tag{10}$$

$$\text{PF} = \cos\left(\arctan\left(\frac{V_d}{V_q}\right)\right) \tag{11}$$

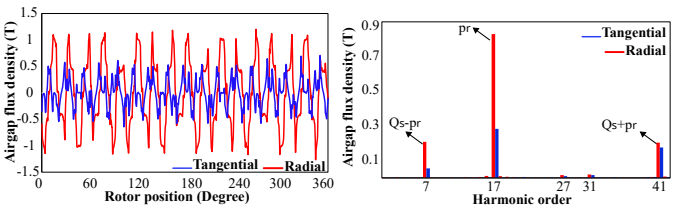

(a) (b)

Fig. 1: Air-gap flux density due to the PM and its FFT. (a) Air-gap flux density, and (b) magnitude of FFT on air-gap flux density.

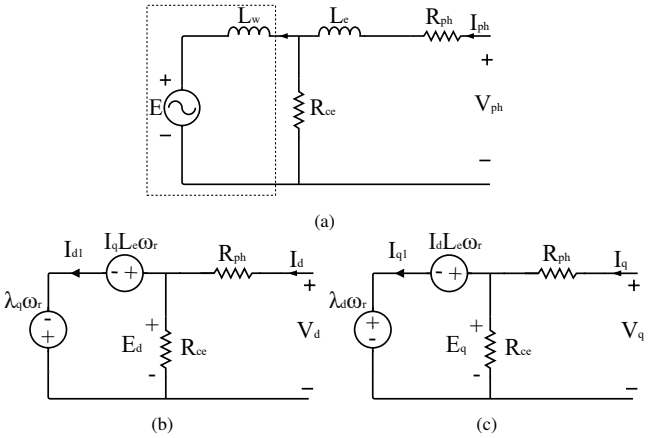

Fig. 2: Equivalent circuits (a) per phase (a) d-axis, and (b) q-axis.

IV. Machine Topology Selection

High pole-ratio PMVMs often suffer from overlapping windings and long end connections due to their limited number of stator pole pairs and larger number of slots [11]. This issue becomes particularly pronounced in machines with a short stack length. To address this challenge, low pole-ratio PMVMs featuring non-overlapping windings have been proposed. However, these machines compromise torque capacity due to a reduced winding factor. The Vernier machine offers an effective solution by employing a FSCW with a coil pitch of two [12]. This approach minimizes end-winding length while maintaining a high winding factor. Based on this rationale, this paper focuses on the design and optimization of a 4.2 kW low pole-ratio ($G_r = 2.4$) FSCW PMVM with a coil pitch of two. Additionally, an open-slot design is employed for the stator to emulate the modulator function of conventional magnetic gear machines, effectively aligning the armature field with the PM magnetic field.

V. Design and Optimization

The 4.2 kW FSCW PMVM was optimized using the NSGA for the D160M frame. The goal of optimization was to effectively reduce the system's cost by minimizing its mass. Therefore, two objective functions with variable dimensions were used to ensure that the dimensions met acceptable performance standards, as shown

$$\min_{X_n}(F(X_n)) = \begin{bmatrix} M_{active}(X_n) \\ M_{PM}(X_n) \end{bmatrix} \tag{12}$$

$$\min_{X_n}(F(X_n)) = \begin{bmatrix} M_{active}(X_n) \\ M_{PM}(X_n) \\ L_{st} \end{bmatrix} \tag{13}$$

$$M_{active} = M_{Fe} + M_{PM} + M_{Cu} \tag{14}$$

$$X_n = \begin{bmatrix} L_{st} & h_{sy} & h_s & g & \alpha & \beta & h_m & h_{ry} \end{bmatrix}, \tag{15}$$

$$X_n = \begin{bmatrix} 60\,\text{mm} \geq L_{\text{st}} \geq 200\,\text{mm} \\ 1\,\text{mm} \geq h_{\text{sy}} \geq 15\,\text{mm} \\ 10\,\text{mm} \geq h_s \geq 50\,\text{mm} \\ 0.3 \geq \alpha \geq 0.75 \\ 0.45 \geq \beta \geq 0.95 \\ 3\,\text{mm} \geq h_m \geq 6\,\text{mm} \\ 3\,\text{mm} \geq h_{\text{ry}} \geq 30\,\text{mm} \\ 1\,\text{mm} \geq g \geq 3\,\text{mm} \end{bmatrix} \tag{16}$$

$$\begin{bmatrix} \text{Output power}\,(P_{\text{out}}) \\ \text{Power factor (PF)} \\ \text{Efficiency}(\eta) \\ \text{Ripple torque} \\ \text{Current density}\,(J_{\text{rms}}) \end{bmatrix} = \begin{bmatrix} 4.2\,\text{KW} \\ \geq 0.7 \\ \geq 94\% \\ \leq 15\% \\ \leq 5\,\text{A/mm}^2 \end{bmatrix} \tag{17}$$

where $\alpha = \frac{\theta_s}{\theta_1}$, $\beta = \frac{\theta_{pm-s}}{\theta_{pm-p}}$, M_{Fe} is the total mass of the stator and rotor iron lamination, M_{Cu} is the total mass of copper, M_{PM} is the total mass of PMs, and L_{st} is the stack length. Fig. 3 depicts all design variables graphically. The results of the optimization, with respect to the objective functions, are shown in Fig. 4 as a Pareto front diagram. It is evident that the results from the two objective functions closely align. All optimal points exhibit a PF value greater than 0.7. The Pareto front diagram depicts all possible design optimizations of the machine that fall within the given constraints. The selection of the optimum machine is made at the knee point of the Pareto front, which is shown in Fig. 4. The optimum structure and dimensions of the optimum machine are shown and presented in Fig. 5 and Table I, respectively.

VI. Electromagnetic Analysis

A. Back EMF and flux

The electromagnetic performance of the proposed PMVM under both no-load and full-load conditions at rated speed was analyzed using the FEM. The total harmonic distortion (THD) of the back EMF was calculated to be 4.4%, indicating the presence of pure sinusoidal and symmetrical waveforms. As shown in Fig. 6, the no-load flux linkage and back EMF waveforms for the three phases of the PMVM can be observed. Fig. 7 illustrates the flux density distribution of the proposed model at full load. It can be observed that the flux densities of the proposed PMVM do not exceed 1.8T.

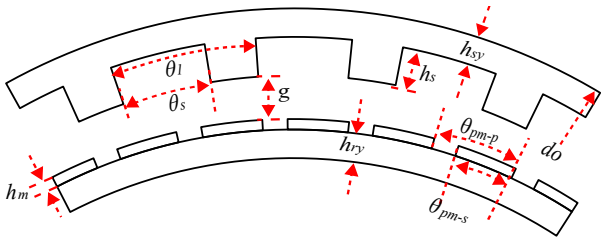

Fig. 3: Graphic representation of design variables.

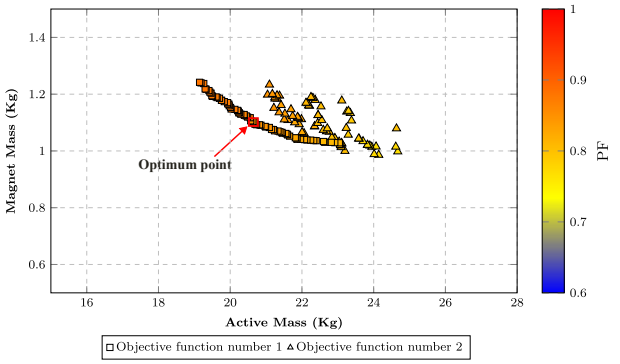

Fig. 4: Pareto front result for two objective functions

TABLE I: The dimensions of optimum 4.2 kW FSCW PMVM with $G_r = 2.4$.

Stator Parameters	Value	Unit
Fill factor	0.4	-
Slot Number	24	-
ps	7	-
Slot area	527	mm^2
Outer diameter	260	mm
Stator bore	190	mm
Slot width (bottom)	20.5	mm
Slot width (top)	16	mm
Slot depth (h_s)	30.5	mm
Slot opening	15.75	mm
Stator yoke (h_{sy})	4.2	mm
Rotor Parameters	**Value**	**Unit**
pr	17	-
Magnet segments radially	3	-
Magnet segments axially	2	-
Magnet arc (θ_{pm-s})	140	degree
Magnet thickness (h_m)	3	mm
Air-gap (g)	1	mm
Inner rotor diameter	172	mm
Rotor yoke (h_{ry})	5.1	mm
Stack length (L_{st})	111.24	mm

B. Torque Characteristics Analysis Based on Flux Modulation Theory

The PMVM's torque-generating mechanism is analyzed based on the established principle of flux modulation. In the PMVM, the interplay between the PMs and the armature reaction magnetic field generates a series of spatial harmonics in the airgap flux density. The proposed PMVM achieves a modulated pole-pair number (PPN) for these space harmonics exclusively through stator tooth modulation. Additionally, the armature reaction magnetic field produces airgap flux density space harmonics. According to classical electromagnetic theory, when the PM magnetic field and armature reaction magnetic field share the same modulated PPN and speed, they interact to produce steady torque. The PMVM's electromagnetic torque is calculated using the Maxwell stress tensor (MST), considering the interaction between the radial and tangential airgap flux-density harmonic components generated by the PMs and the stator winding.

$$T = \sum_{v=1}^{\infty} kB_{rv}B_{tv}\cos(\theta_{rv} - \theta_{tv}) \tag{18}$$

where, θ_{rv} and θ_{tv} represent the angle of the radial and tangen-

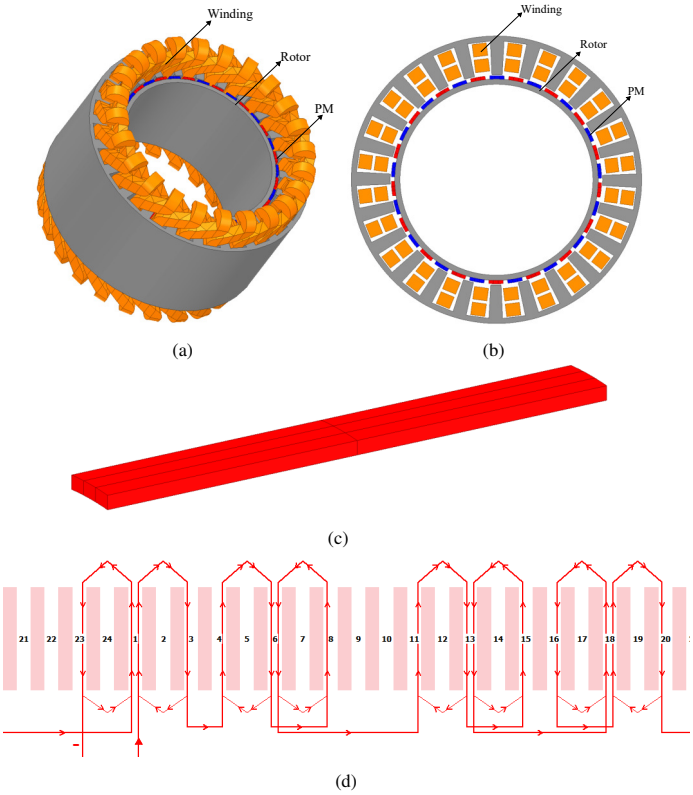

Fig. 5: Optimum structure (a) 3D (b) 2D, (c) segmented PM, and (d) linear pattern of winding connection for one phase.

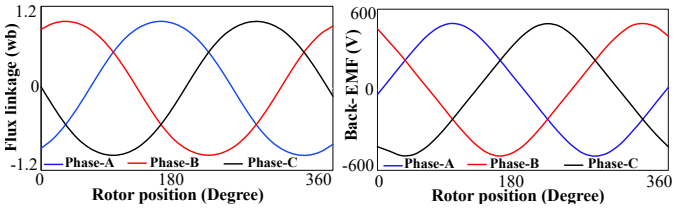

Fig. 6: (a) flux linkage and, (b) back EMF.

tial air-gap flux densities, respectively. The torque contribution of each harmonic in the proposed model was computed using the MST and is summarized in Table II. Analysis of Table II reveals that several harmonics play a role in torque generation in the PMVM. Notably, the 17th harmonic (p_r^{th}) emerges as the

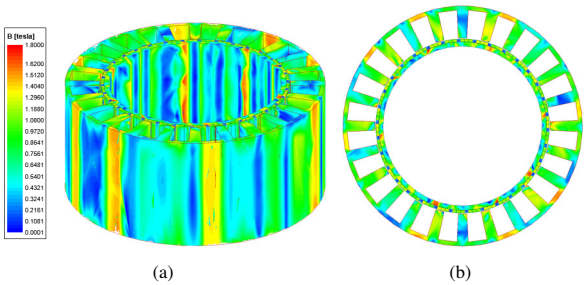

Fig. 7: airgap flux density comparison. (a) 3D (b) 2D.

TABLE II: Percentage contribution of the PMVM to harmonic torque.

v	$B_r(T)$	$B_t(T)$	$Cos(\theta_r - \theta_t)$	T (%)
7	0.2	0.05	0.038	**1%**
17	0.83	0.28	0.22	**97%**
27	0.015	0.01	0.3	0.1%
41	0.2	0.17	0.0078	0.6%
55	0.05	0.05	0.02	0.13%
89	0.04	0.04	0.04	0.17%

predominant contributor to torque production. Fig. 8 depicts the profiles of steady-state rated torque and cogging torque for the PMVM. It can be observed that the ripple torque of the proposed model is low, measuring at 3.5%.

VII. Mechanical and Thermal Feasibility

The machine excels in electromagnetic performance but needs a closer examination of its mechanical layout, with a specific focus on thermal considerations in its construction.

A. Force and deflection

Unbalanced magnetic forces (UMF) in a PMVM can originate from diverse factors, posing the risk of mechanical stress, vibrations, and a shortened motor lifespan. Therefore, it is crucial to minimize these forces to the greatest extent possible [13]. While the PMVM was designed to be balanced, it remains essential to conduct thorough checks on the forces to guarantee smooth operation during the machine's construction Eqns (19) and (20) are defined to ensure that the machine is balanced theoretically and the proposed PMVM fulfills these criteria. The UMF is illustrated in Fig. 9(a), and it is evident that the average UMF is 11 N, which is considered low and acceptable.

$$gcd(2p_r, Q_s) \geq 2 = gcd(2 * 17, 24) = 2 \quad (19)$$

$$gcd(2p_s, Q_s) \geq 2 = gcd(2 * 7, 24) = 2 \quad (20)$$

The interaction between the rotor and stator magnetic fields generates an electromagnetic attraction force, leading to deformation and stress in the stator back iron and frame. These forces result from the pressure exerted by the magnetic field strength relative to the permeability of free space. The electromagnetic attraction force can be calculated as follows

$$F_r = \frac{1}{2\mu_0}(B_r^2 - B_t^2) l_{stk} l_{arc} \quad (21)$$

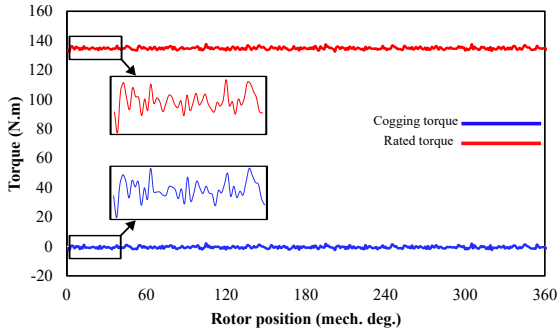

Fig. 8: Rated torque and cogging torque.

$$F_t = \frac{1}{\mu_0}(B_r B_t) l_{stk} l_{arc} \tag{22}$$

$$F_T = \sqrt{F_r^2 + F_t^2} \tag{23}$$

where, l_{stk}, l_{arc} is the stack length and length of arc over the stator teeth of the proposed PMVM. Since tangential forces are relatively small, the majority of attraction forces act in the radial direction. According to the provided formula, the calculated attraction force in the PMVM is 250 N per stator tooth as can be seen in Fig.9 (b). FEM conducted in Ansys mechanical illustrates the distribution of attraction forces across the proposed PMVM. These forces have the potential to induce stress in the stator teeth and affect the bolts securing the stator to the frame. Consequently, a stress analysis is imperative to verify that the bolts can withstand the attraction forces and prevent stator deformation. In Fig. 10 (a), the mechanical assembly of the PMVM and the stress analysis on the stator are depicted. Assuming a uniform area and considering a reliability factor, the maximum stress on the stator and rotor is calculated to be 27.3 MPa and 13.8 MPa, respectively. This corresponds to safety factors of 11 and 22, respectively. These results suggest that the stator and rotor yoke are adequately thick to withstand the attraction force generated by the machine. The maximum deflection occurs at the peak stress state, with the stator and rotor laminations deflecting approximately 0.0152 mm and 0.00281 mm, respectively, in the radial direction at maximum load. This deflection is acceptable for a machine with a 1 mm air gap. Therefore, the attraction force will not hinder the machine's normal operation.

B. Thermal analysis

Thermal analysis is essential for electrical machines because it helps them run safely and efficiently. Heat is produced inside the PMVM due to losses, and this heat needs to be removed to prevent the machine from getting too hot and damaging its parts. By carefully checking the temperature distribution, it can be decided if a cooling system needs to be added to take away the extra heat. This paper employs the Lumped Parameter Thermal Model (LPTM), implemented within Motor-Cad software, to perform thermal analysis of the PMVM in the absence of any cooling system, enabling a comprehensive evaluation of component temperatures under natural convection conditions. As depicted in Fig 11, the

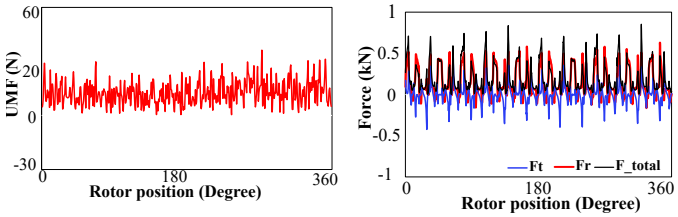

(a) (b)

Fig. 9: Forces. (a) UMF force, and (b) attraction force.

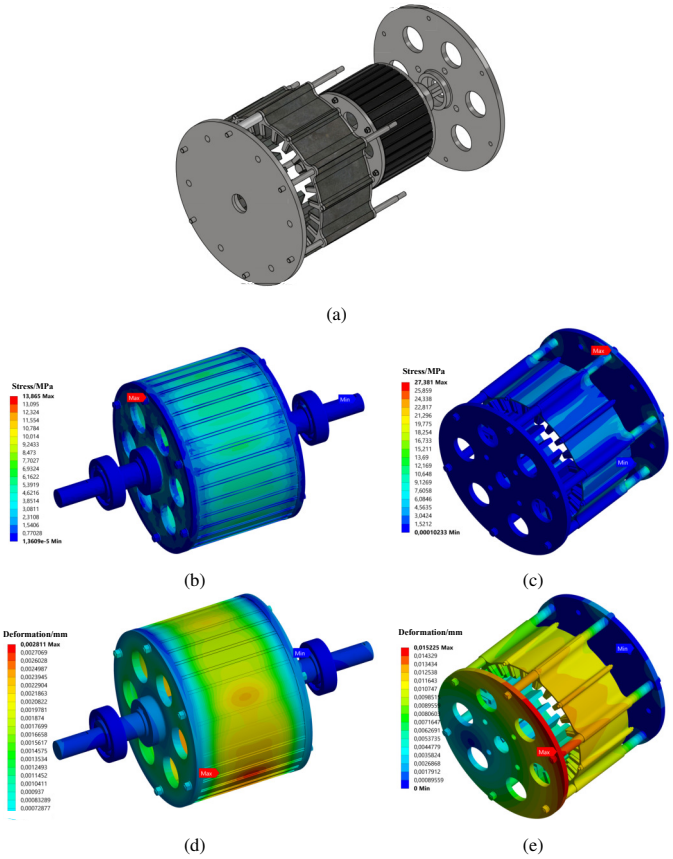

(a) (b) (c) (d) (e)

Fig. 10: (a) Mechanical assembling (b) rotor stress, (b) stator stress, (b) rotor deformation, and (b) stator deformation.

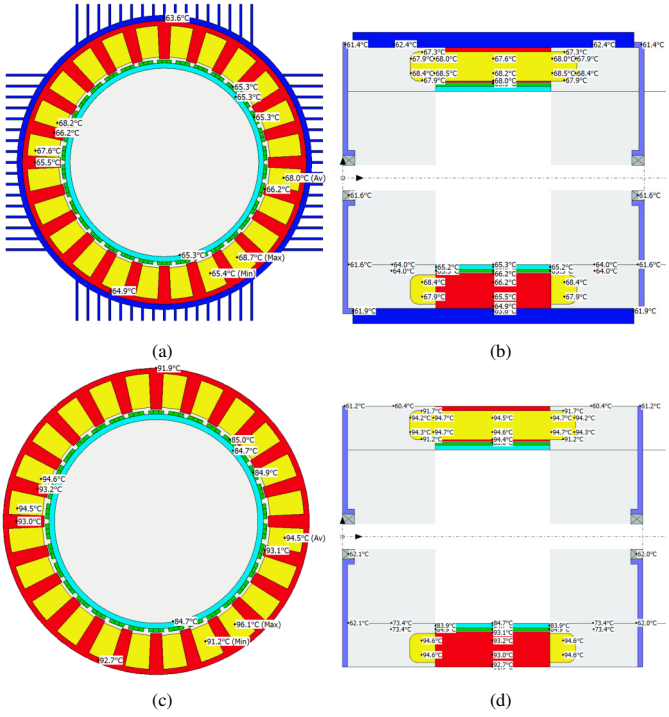

(a) (b) (c) (d)

Fig. 11: Thermal analysis (a) radial perspective with fins (b) axial perspective with fins, (b) radial perspective without fins, and (b) axial perspective without fins.

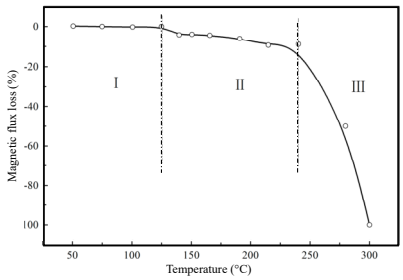

Fig. 12: Thermal demagnetization curve of PM.

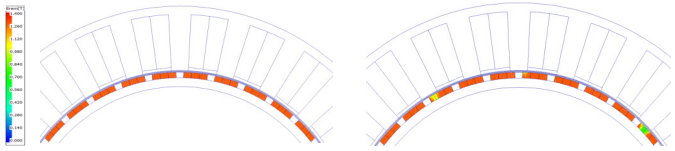

(a) (b)

Fig. 13: Demagnetization analysis of (a) steady-state, and (b) short-circuit condition.

maximum temperatures in the steady-state for the end winding with and without fins, are 68.5°C and 94.6°C, respectively. The temperatures for the magnets with and without fins are 65.3°C and 85°C, which fall within acceptable limits. According to the observations in Fig. 12, the magnetic properties of the PM remain essentially unchanged for temperatures below the maximum working temperature of approximately 120°C. Consequently, there is no demagnetization, and the PMVM operates optimally. Demagnetization is specifically considered and analyzed in the proposed models under the highest operating temperature of steady-state and short-circuit conditions. As depicted in Fig. 13 (a), there is no indication of demagnetization in the PM. However, under short-circuit conditions as shown in Fig. 13 (b), a small portion of the magnets experiences demagnetization. For an overall overview of the performance of the proposed model, all electromagnetic parameters and key criteria are summarized in Table III.

TABLE III: Electromagnetic performance of proposed PMVM.

Parameters	**Value**
Frequency (Hz)	85
Stator mass (kg)	9.6
Rotor mass (kg)	2.2
Copper mass (kg)	7.6
PM mass (kg)	1.1
Current dens. (A/mm^2)	3.6
Power factor (PF)	0.88
Efficiency (%)	92.5
Core loss (W)	66
Magnet loss (W)	3.5
Copper loss (W)	263
Rated torque (Nm)	133
Ripple torque (%)	3.5
Torque per volume (KNm/m^3)	22.5
Torque per active mass (Nm/kg)	6.2

VIII. Conclusion

This paper presents the design and optimization of a low pole ratio FSCW PMVM with a coil pitch of two for direct drive applications. The proposed motor was comprehensively evaluated in terms of its electromagnetic performance, forces, mechanical aspects, thermal characteristics, and demagnetization susceptibility to ensure the validity of the proposed model. The results indicate that the proposed FSCW PMVM showcases notable characteristics, including high power density, low torque ripple, high PF, exceptional thermal performance, and enhanced energy efficiency. These features collectively position it as a cost-effective, reliable, and environmentally friendly solution for direct drive applications.

References

[1] V. Teymoori, N. Eskandaria, N. Arish and A. Khalili, "Design of permanent magnetic motor speed controller drive with power supply inverter based on a new switching method," 2019 International Power System Conference (PSC), Tehran, Iran, 2019, pp. 453-458.

[2] N. Arish, M. J. Kamper and R. -J. Wang, "Electromagnetic Analysis of Flux Barrier U-Shaped Permanent Magnet Vernier Motor," 2021 International Aegean Conference on Electrical Machines and Power Electronics (ACEMP) and 2021 International Conference on Optimization of Electrical and Electronic Equipment (OPTIM), Brasov, Romania, 2021, pp. 198-204.

[3] B. Kim and T. A. Lipo, "Operation and Design Principles of a PM Vernier Motor," in IEEE Transactions on Industry Applications, vol. 50, no. 6, pp. 3656-3663, Nov.-Dec. 2014, doi: 10.1109/TIA.2014.2313693.

[4] N. Arish, M. J. Kamper and R. -J. Wang, "Performance of Large Low-Pole-Ratio Non-Overlap-Winding PM Vernier Motor," 2023 26th International Conference on Electrical Machines and Systems (ICEMS), Zhuhai, China, 2023, pp. 5255-5260.

[5] N. Arish, M. Ardestani and V. Teymoori, "Comparison of Dual Stator Consequent-pole Linear Permanent Magnet Vernier Machine with Toroidal and Concentrated Winding," 2020 11th Power Electronics, Drive Systems, and Technologies Conference (PEDSTC), Tehran, Iran, 2020, pp. 1-5.

[6] N. Arish, V. Teymoori, H. Yaghobi and M. Moradi, "Design of New Linear Vernier Machine with Skew and Halbach Permanent Magnet for Wave Energy Converters," 2019 International Power System Conference (PSC), Tehran, Iran, 2019, pp. 90-94.

[7] N. Arish, H. Yaghobi and V. Teymoori, "Optimization and Comparison of New Linear Permanent Magnet Vernier Machine," 2019 27th Iranian Conference on Electrical Engineering (ICEE), Yazd, Iran, 2019, pp. 657-661.

[8] N. Arish, "Electromagnetic Performance Analysis of Linear Vernier Machine with PM and HTS-Bulk", Phys. C Supercond. its Appl, vol. 579, 2020.

[9] T. Zou, D. Li, R. Qu, D. Jiang and J. Li, "Advanced High Torque Density PM Vernier Machine With Multiple Working Harmonics," in IEEE Transactions on Industry Applications, vol. 53, no. 6, pp. 5295-5304, Nov.-Dec. 2017.

[10] B. Kim and T. A. Lipo, "Operation and Design Principles of a PM Vernier Motor," in IEEE Transactions on Industry Applications, vol. 50, no. 6, pp. 3656-3663, Nov.-Dec. 2014.

[11] Xu, L., Liu, G., Zhao, W., Ji, J., Zhou, H., Zhao, W., et al.: 'Quantitative comparison of integral and fractional slot permanent magnet vernier motors', *IEEE Transactions on Energy Conversion*, 2015, **30**, (4), pp. 1483–1495

[12] N. Arish, M.J. Kamper and R.-J. Wang, "Performance Comparison of 5-MW Normal and Dual Three-Phase PM Vernier Motors for Ship Propulsion,"2023 Int. Aegean Conf. on Electrical Machines and Power Electronics (ACEMP) & 2023 Int. Conf. on Optimization of Electrical and Electronic Equipment (OPTIM), 2-3 Sept. 2021, Istanbul, Turkey, pp. 1-8.

[13] Y. Lu, J. Li, R. Qu, D. Ye and H. Lu, "Electromagnetic Force and Vibration Study on Axial Flux Permanent Magnet Synchronous Machines With Dual Three-Phase Windings," IEEE Transactions on Industrial Electronics, 67(1): 115-125, 2020.